

Earth's topographic relief potentially limited by an upper bound on channel steepness

George E. Hilley^{1*}, Stephen Porder², Felipe Aron³, Curtis W. Baden¹, Samuel A. Johnstone^{1,4}, Frances Liu¹, Robert Sare¹, Aaron Steelquist¹ and Holly H. Young¹

Rivers limit the maximum elevation of active mountain belts, control the coupling between climate and tectonic processes, and archive the pace and tempo of fault-related rock uplift rates. Topographic profiles along rivers in steep, non-glaciated landscapes have led many to posit that river incision rates vary as a power function of channel discharge and slope. We used ¹⁰Be abundance in river sands and topographic analysis to test this relationship in watersheds varying by four orders of magnitude in erosion rate (4.7×10^{-3} – 7.1 mm yr^{-1}), and supplemented this with a global analysis of erosion rates and topography. Our data and analyses reveal that in steep, rapidly eroding landscapes, channel morphology does not scale with erosion rate as expected. Instead, river profiles reach a threshold steepness, which may provide a bound on the topographic relief of Earth. In this case, increases in channel length may limit topographic relief, as erosion rate becomes increasingly sensitive to small changes in channel slopes in steep landscapes.

Decades of research builds on the premise that topographic relief across Earth's non-glaciated surface is limited by the rate at which rivers incise into bedrock, ε [L/t] (ref. ¹). The response of ε to factors such as climate, water discharge and channel slope fundamentally controls the sensitivity of landscapes to climate changes^{1–4}, tectonic motions⁵ and the properties of different rocks exposed at Earth's surface. The rate of incision, in turn, is thought to increase with the shear stress or unit stream power that a river exerts on its bed^{6,7}. Under idealized circumstances, this leads to a prediction that ε is related to a river's slope (S ; [°]) and upstream catchment area (A ; [L²])^{7,8} as a power function, hereafter referred to as the power-law incision rule:

$$\varepsilon = KA^m S^n \quad (1)$$

where m and n are scaling exponents whose ratio m/n (θ ; [°]) is typically 0.4–0.6 (refs. ^{7,9,10}) and K [L^{1–2 θ} /t] captures erosivity (a function of rock type, climate and downstream changes in channel hydraulic geometry^{7,10–12}). Channel steepness (k_s ; [L^{2 θ}]) in turn normalizes channel slope for catchment area and can be directly measured from digital elevation models (DEMs)^{5,13} as:

$$k_s = A^{(m/n)} S \quad (2)$$

The application of the power-law incision rule relates the channel incision rate (ε) to k_s , rock properties and some information about incisional mechanics (manifest in n)¹⁴ as:

$$k_s = \left(\frac{\varepsilon}{K}\right)^{1/n} \quad (3)$$

Thus, in catchments where K can be regarded as constant (by controlling for rock type and climate) and ε has been measured (in this work, using the abundance of cosmogenic radionuclides in

river sands¹⁵), the power-law incision rule requires that co-located measurements of the logarithms of ε and k_s plot along a straight line. The slope of the line in this plot is $1/n$, while the ordinate intercept is the logarithm of $K^{-1/n}$ given that n is constant across all incision rates, catchment lithologies and climates.

Power-law incision model in tropical granitic landscapes

While the power-law incision model has long been used, it has never been tested across a spectrum of ε that spans a broad (>3 orders of magnitude) range of tectonic landscapes, while controlling for other factors. Thus, we selected 14 basins of varying tectonic activity from 5 tropical landscapes (mean annual precipitation between 1.5 and 3 m yr⁻¹), underlain by granitic bedrock, to empirically determine the relationship between ε and k_s (see Supplementary Information). The restriction to tropical landscapes and uniform lithology allowed us to avoid formerly glaciated landscapes that would invalidate tests of the power-law incision rule and control for confounding factors encapsulated in K . This approach contrasts with previous global analyses of ε and k_s (ref. ¹⁶), which subsume a variety of rock types and climates that may exert control on channel steepness, independent of incision rate¹¹.

We measured ε and k_s using ¹⁰Be-determined erosion rates in sampled river sands (for ε) and analysis of DEMs at each site (using the SRTM-v4 90-m elevation model to calculate k_s ; methods of analysis and results of tests of the impact of resolution on topographic analysis are described in Supplementary Information; Supplementary Tables 1–3; code repository at <https://github.com/stgl/TopoAnalysis> and <https://github.com/stgl/GlobalSteepness>; all data generated and analysed during this study are available from the corresponding author on reasonable request). Following previous studies^{16–20}, we assumed that erosion rates across an entire catchment are uniform and reflect the incision of bedrock channels. Many of the sampled catchments are steep, which promotes a degree of mass failure or nonlinear hillslope transport. Both of these

¹Department of Geological Sciences, Stanford University, Stanford, CA, USA. ²Department of Ecology and Evolutionary Biology, Brown University, Providence, RI, USA. ³National Research Center for Integrated Disaster Risk Management (CIGIDEN) & Departamento de Ingeniería Estructural y Geotécnica, Pontificia Universidad Católica de Chile, Santiago, Chile. ⁴Present address: United States Geological Survey, Lakewood, CO, USA.

*e-mail: hilley@stanford.edu

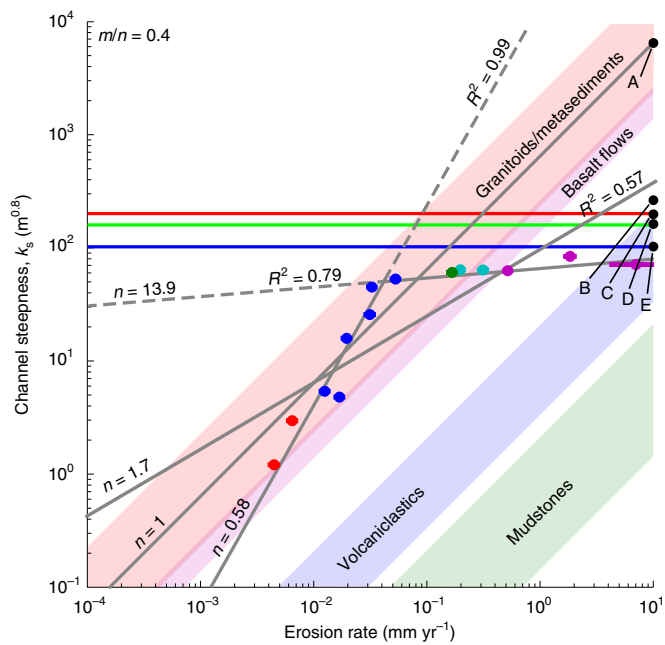


Fig. 1 | ^{10}Be -measured erosion rates and channel steepness from tropical granitic landscapes. ^{10}Be -measured erosion rates and k_s values observed in Venezuela (red), Brazil (blue), Guatemala (green), Costa Rica (cyan) and Taiwan (purple) sampling sites for $m/n=0.4$ (for comparison to previous work¹¹). The horizontal error bars represent 1σ analytical errors of erosion rates. The results for other m/n values are shown in Supplementary Information. The horizontal blue, green and red lines reference $k_s=100$, 150 and $200\text{ m}^{0.8}$, respectively, which are also shown in Fig. 2. The coloured fields bound relationships between ε and k_s for different rock types (represented by values of K in equation (1)) for $n=1$ (ref. ¹¹). The grey lines highlight fits to equation (3) for different values of n . A–E, reference k_s values used in the calculations shown in Fig. 4.

processes cause hillslopes to rapidly adjust to changes in channel incision rates, which allows us to equate catchment-averaged erosion rate and ε (see Supplementary Information). The ^{10}Be data reveal that our sampling spanned four orders of magnitude variation in ε (Fig. 1), ranging from $4.7 \times 10^{-3}\text{ mm yr}^{-1}$ at the lowest-relief site (Guyanan Shield in Venezuela) to 7.1 mm yr^{-1} at the highest-relief site (Taiwan). In the low-relief catchments of Venezuela and Brazil, ε increased with k_s . This relationship implies $n=0.58 \pm 0.07$ ($R^2=0.99$; $m/n=0.4$) and K from 5.4×10^{-6} to $2.6 \times 10^{-5}\text{ m}^{0.2}\text{ yr}^{-1}$ (calculated using $n=1$, $m/n=0.4$ for comparison with previous work¹¹), which is consistent with expectations for granitic landscapes¹¹. However, in steeper basins ($k_s \gtrsim 60\text{ m}^{0.8}$), ε was far more sensitive to k_s over a two order of magnitude range in ε ($n=13.9 \pm 8.4$; $R^2=0.79$) and k_s did not exceed $\sim 80\text{ m}^{0.8}$.

While a simple power law adequately characterized the relationship between ε and k_s in low-steepness landscapes, we observed a nearly constant k_s that appeared decoupled from ε at higher erosion rates. This stands in contrast to the assumptions of previous studies, which sampled either across a range of lithologies and climates and/or over a limited range of erosion rates^{16,18,21}. If we combine and regress data from our sampled sites, we infer $n=1.7$ ($R^2=0.57$; Fig. 1), similar to regressions of global compilations that assume that the power-law incision rule is applicable over the entire range of incision rates¹⁶. Likewise, if we filter these global compilations to isolate similar lithologies and climatic conditions as our sites, available measurements are clustered around two distinct, smaller ranges of ε , whose paired values are consistent with those we measured (Supplementary Fig. 2). Regressing to infer n using these

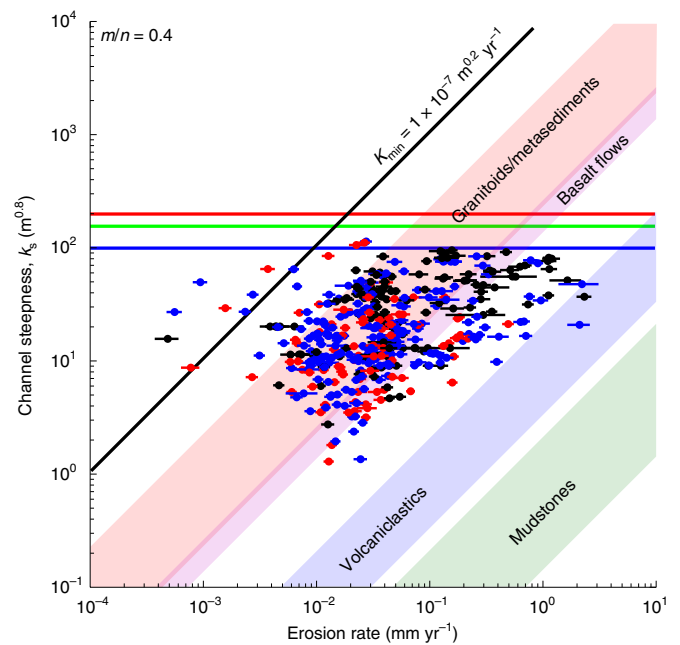


Fig. 2 | Global occurrence of ^{10}Be erosion rates and channel steepness.

Global compilation of ^{10}Be -measured erosion rates²³ and k_s (ref. ²⁴). The data are coloured on the basis of the R^2 values for the correlation between relief and χ (for definition of χ , see equation (4), Methods). The red, blue and black points have R^2 values >0 , 0.7 and 0.9 , respectively. The horizontal errors represent 1σ analytical errors of erosion rates. The maximum k_s value observed in the compilation is $112\text{ m}^{0.8}$, despite predictions of k_s as high as $\sim 1 \times 10^4\text{ m}^{0.8}$ based on inferred K values for $n=1$, $m/n=0.4$ (ref. ¹¹). ε - k_s pairs generally plot within rock types composed of incisionally resistant lithologies, which may reflect the absence of 250–500 μm quartz crystals in mudstones, which may be limited by the ability of channels to transport sediment, which provides a lower limit to k_s .

isolated, clustered measurements results in a constant value of $n=2$ (refs. ^{16,18,21}). This raises the possibility that the threshold we detected may also be present within global compilations of ε and k_s . As such, previous inferences of the scaling between ε and k_s may reflect the assumption that the power-law incision model is applicable across the full range of ε that is globally observed. If this is the case, our carefully selected, systematic and controlled sampling across a large gradient in ε resolved a fundamental change in the way in which k_s scales with ε that is not captured by the power-law incision rule.

Global channel steepness limit

To determine whether the threshold we observed along our controlled gradient in ε is a worldwide phenomenon, we analysed global compilations of ^{10}Be -derived erosion rates. These compilations cannot be used to directly test the power-law incision rule because the primary studies did not control for other factors that influence K . Nonetheless, equation (3) indicates that measured values of k_s should be less than ε/K_{\min} , where K_{\min} is the minimum reported calibrated value for K (regarded in this study as the order of magnitude of the lowest reported value; $K_{\min}=1 \times 10^{-7}\text{ m}^{0.2}\text{ yr}^{-1}$ for $m=0.4$, $n=1$)¹¹. Thus, if the power-law incision rule is applicable across all of Earth's non-glaciated landscapes, values of ε and k_s should plot below the bound represented by K_{\min} (Fig. 2). Furthermore, if the k_s threshold that we detected within our sampled basins is present globally, all measured ε - k_s pairs must plot below the threshold k_s value. This is despite the fact that the power-law incision rule predicts k_s values that are two orders of magnitude greater than the threshold value within rapidly ($>1\text{ mm yr}^{-1}$) eroding landscapes (for

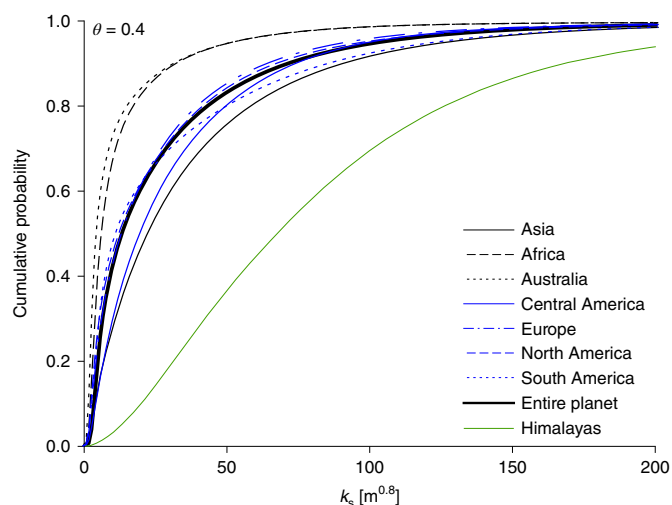


Fig. 3 | Global distribution of channel steepness. Cumulative distribution plots of k_s for $m/n=0.4$ (see Supplementary Information for cumulative distribution functions using $m/n=0.5, 0.6$). Fewer than 1% of all points across the planet show k_s values $>200\text{ m}^{0.8}$, regardless of whether they were recently glaciated.

example, the Himalayas²²; Figs. 1 and 2) underlain by rock types resistant to incision (granitoids and metasediments¹¹; Figs. 1 and 2) when $n=1$ (ref. ¹¹). Assuming $n=2$, as has been previously done for global compilations¹⁶, produces k_s values that exceed the k_s threshold by an order of magnitude under these conditions. These large expected discrepancies between predictions of the power-law incision rule and our limiting k_s threshold should be resolvable even within global compilations that do not control for factors such as climate and rock type.

We used a global compilation of ¹⁰Be-derived values of erosion rate to estimate ε (ref. ²³) with global DEMs²⁴ (HydroSheds 500-m-resolution elevation models) to calculate k_s for large ($>5\text{ km}^2$) basins within this dataset that did not show morphologic evidence of recent glacial erosion (Supplementary Information). Most (98.5%) of the k_s values plotted below the bound defined by K_{\min} . Those basins that fell outside this range were almost exclusively located in the landscapes of the Atacama Desert and Namibia (Supplementary Information). Outside these extreme cases, limits to k_s in slowly eroding landscapes ($<3 \times 10^{-3}\text{ mm yr}^{-1}$) appeared consistent with those expected from the power-law incision model (Fig. 2). In contrast, controls on k_s in rapidly eroding landscapes were not captured by the power-law incision rule (Fig. 2). Instead, across all erosion rates k_s was less than $112\text{ m}^{0.8}$ (this value increases with the reference concavity used; Supplementary Information), even within basins experiencing rapid erosion. In the most rapidly eroding basin ($\varepsilon=3.66\text{ mm yr}^{-1}$) contained within this global compilation, we would expect k_s as high as $\sim 832\text{ m}^{0.8}$ for $K=4.4 \times 10^{-7}\text{ m}^{0.2}\text{ yr}^{-1}$ (calibrated K values for $n=1, m=0.4$; ref. ¹¹), which is not observed. Even in the case of $n=2$, k_s values expected from the power-law incision rule overestimate the observed k_s . Thus, large k_s values predicted by the power-law incision rule appear truncated by a threshold similar in value to that we observed (Fig. 1).

As a final test that k_s and ε do not follow the power-law incision rule at high erosion rates, we expanded our analysis beyond basins for which ¹⁰Be data exist to constrain ε . We used global DEMs²⁴ to test whether the limiting value of $k_s \cong 112\text{ m}^{0.8}$ bounds relief on Earth. To do this, we calculated k_s values across Earth's surface, and determined cumulative distribution functions (CDFs) of this value for each continent individually, and for the planet as a whole (Fig. 3 and Supplementary Information). k_s values were calculated at the

centre of river segments along which the elevation drop exceeded 48 m, which is three times the reported vertical precision of the elevation measurements from which the HydroSheds 500-m-resolution data were derived²⁴ (Methods). For each valid segment, we calculated the integrated $A^{-\theta}$ value along each point of the segment, and regressed these values with the segment's elevation drops to calculate k_s (ref. ¹³).

We used this plot to determine how much of Earth's topography is characterized by steepness values below specified k_s thresholds (Fig. 3). We found that only 4.0% of points on Earth show $k_s > 112\text{ m}^{0.8}$ (most areas meeting this condition show morphologic evidence of recent glacial activity). Furthermore, only $<0.8\%$ of points on the planet displayed $k_s > 200\text{ m}^{0.8}$, and even that value is approximately two orders of magnitude lower than the range expected assuming a power-law incision rule with $m=0.4, n=1$ (refs. ^{10,11}), $\varepsilon=10\text{ mm yr}^{-1}$ and $K=4.4 \times 10^{-7}\text{ m}^{0.2}\text{ yr}^{-1}$. Even when isolating measurements from the Himalayas, where high erosion rates have exposed resistant rocks in places and where glacial processes may play an important role in determining landscape steepness, points with $k_s > 200\text{ m}^{0.8}$ are rare ($<6\%$; Fig. 3). When calculating the average k_s value within worldwide basins whose watershed area is within a factor of two of the median watershed area of compiled basins²³ (157.5 km^2 ; Supplementary Table 4), we found that only 0.1% of all basins displayed average $k_s > 112\text{ m}^{0.8}$ and none of these basins showed average $k_s > 200\text{ m}^{0.8}$.

Implications of a limiting threshold of channel steepness

The power-law incision rule places constraints on global channel relief observed on Earth because this relief is predicted to scale with $k_s, m/n$, rock uplift rate (here assumed equal to ε for steady-state landscapes) and along-channel length (because catchment area increases with downstream distance¹). Should k_s attain a maximum of $4,466\text{ m}^{0.8}$ as would be expected from the extrapolation of the power-law incision rule where $n=1$ to high (10 mm yr^{-1}) incision/rock uplift rates (point A in Fig. 1), even small basins with channel lengths of 30 km would produce $>140\text{ km}$ of channel relief (Fig. 4), which is clearly not observed on Earth. Furthermore, the steep channels in such a landscape would probably be dominated by non-fluvial mass transport throughout their length²⁵. Even for $k_s=290\text{ m}^{0.8}$, which would be expected at high uplift rates when $n=2$, channel relief in these small basins would reach 10 km, which is about twice the total channel relief that is globally observed. However, a simple limit in which $k_s \leq 100\text{ m}^{0.8}$ successfully reproduces the magnitude of channel relief typical of the steepest of the narrow, ocean-draining mountain belts on Earth (such as the Central Mountain Range of Taiwan). When viewing the global distribution of k_s (Fig. 3), this same channel steepness threshold also bounds the overall topographic relief on our planet to the observed range. Thus, this k_s threshold may place a fundamental limit on the amount of channel relief that can be generated on Earth.

This k_s threshold is not easily captured by our current understanding of channel incision processes^{1,5-8,10,14,18,26}. We observed that the fraction of the channel network with slopes >0.2 , which is thought to reflect the conditions under which channel incision gives way to debris flow processes²⁵, increases similarly to k_s (Supplementary Information). However, it is unclear whether this correspondence implies that debris-flow processes limit channel steepnesses by enhancing erosion, or simply reflects triggering of debris flows as landscape slopes steepen. Furthermore, higher peak discharges that take place in high-relief areas may play an important role in enhancing channel erosion and suppressing channel steepness, although, at least within our sites, this effect may be insufficient to explain the magnitude of channel steepnesses that we observed (Supplementary Information). Indeed, the limit to channel steepness observed within the global erosion-rate dataset spans

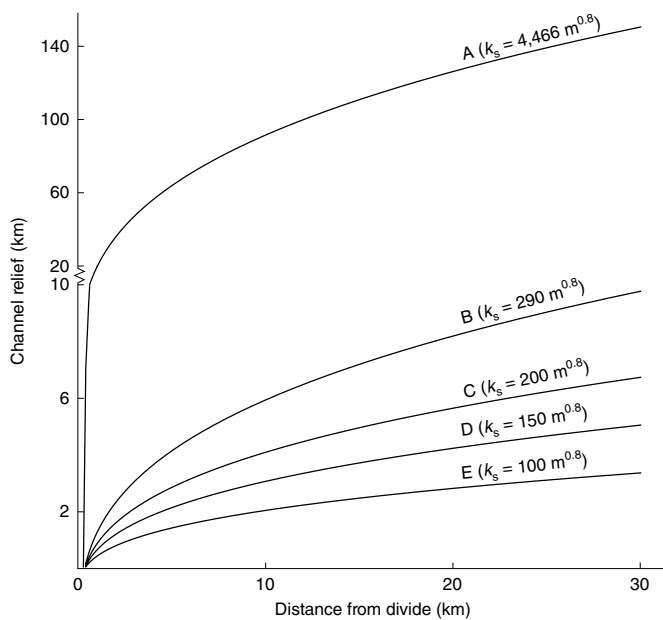


Fig. 4 | Channel relief and steepness predicted by the power-law incision model. Maximum relief predicted by the power-law incision rule for the k_s conditions denoted A–E in Fig. 1. The calculations and the horizontal axis range are based on previous work¹ using $m/n=0.4$, $k=6.7^{12}$ and $h=1.65^{12}$, where $A=kl^h$ (l is the downstream channel length). Even in these small basins, extrapolation of the power-law incision rule to high ϵ , low K conditions when $n=1$ (A) or $n=2$ (B) yields ≥ 2 times the total channel relief observed on Earth, while k_s values close to the observed threshold (D, E) match the observed maximum channel relief.

a range of environmental conditions, suggesting that climatic variation, in itself, may be insufficient to explain the limit we observed. Alternatively, channel-width adjustments²⁷ and bed-cover effects²⁶ might limit k_s in these steep landscapes in a way that is not yet acknowledged. Another possibility is that the slopes of mountainous channels are limited by the size of transported sediment, which may cause erosion rates to become progressively more sensitive to channel slopes as landscapes become steeper²⁸.

There are several fundamental implications of the observed limit on channel steepness and relief. Tectonically active mountain belts typically generate rock uplift rates on the order of 1–10 mm yr⁻¹, and often expose crystalline basement rocks after supracrustal sediments have been exhumed. The results of this analysis imply that large rock uplift and erosion rates can maintain k_s near its limiting value, and thus sustain near-constant orogen relief, despite changes in erosivity that might be expected from the exhumation of more resistant rocks or as a result of Pliocene cooling¹. The corollary to this is that the response of such landscapes to changes in tectonic rates could be quite rapid²⁹, allowing erosion rates in many active landscapes to closely track the rate of material supplied by uplift¹⁷. Furthermore, a large and growing body of work has used k_s (or derivative quantities) to infer variations in tectonic uplift rates across active mountain belts⁵. Many of these landscapes are located in areas close to or at the limiting k_s value. The k_s limit reduces information contained within the channel geometry of these landscapes; instead, sampling erosion rate may be a more reliable means of inferring spatial variations in tectonic uplift rates^{17,30}. Finally, a limit on k_s implies that the widths of active orogens may place a bound on the channel relief in non-glaciated landscapes of our planet. This may contribute to the observed limit on Earth's current topography (<5.5 km of channel relief), and may constrain the plausible elevations of past mountain belts.

Online content

Any methods, additional references, Nature Research reporting summaries, source data, statements of code and data availability and associated accession codes are available at <https://doi.org/10.1038/s41561-019-0442-3>.

Received: 11 June 2018; Accepted: 2 August 2019;

Published online: 16 September 2019

References

- Whipple, K. X., Kirby, E. & Brocklehurst, S. H. Geomorphic limits to climate-induced increases in topographic relief. *Nature* **401**, 39–43 (1999).
- Willett, S. D. Orogeny and orography: the effects of erosion on the structure of mountain belts. *J. Geophys. Res.* **104**, 28957–28981 (1999).
- Hilley, G. E., Strecker, M. R. & Ramos, V. A. Growth and erosion of fold-and-thrust belts with an application to the Aconcagua fold-and-thrust belt, Argentina. *J. Geophys. Res.* **109**, B01410 (2004).
- Whipple, K. X. & Meade, B. J. Controls on the strength of coupling among climate, erosion, and deformation in two-sided, frictional orogenic wedges at steady state. *J. Geophys. Res.* **109**, F01011 (2004).
- Wobus, C. et al. Tectonics from topography: procedures, promise, and pitfalls. *Geol. Soc. Am. Spec. Pap.* **398**, 55–74 (2006).
- Seidl, M. A. & Dietrich, W. E. The problem of channel erosion into bedrock. *Funct. Geomorphol.* **23**, 101–124 (1992).
- Howard, A. D. & Kerby, G. Channel changes in badlands. *Geol. Soc. Am. Bull.* **94**, 739–752 (1983).
- Howard, A. D. A detachment-limited model of drainage basin evolution. *Water Resour. Res.* **30**, 2261–2285 (1994).
- Flint, J. J. Stream gradient as a function of order, magnitude, and discharge. *Water Resour. Res.* **10**, 969–973 (1974).
- Whipple, K. X. & Tucker, G. E. Dynamics of the stream-power river incision model: implications for height limits of mountain ranges, landscape response timescales, and research needs. *J. Geophys. Res.* **104**, 17661–17674 (1999).
- Stock, J. D. & Montgomery, D. R. Geologic constraints on bedrock river incision using the stream power law. *J. Geophys. Res. B* **104**, 4983–4993 (1999).
- Hack, J. T. *Studies of Longitudinal Stream Profiles in Virginia and Maryland* (US Government Printing Office, 1957).
- Perron, J. T. & Royden, L. An integral approach to bedrock river profile analysis. *Earth Surf. Process. Landf.* **38**, 570–576 (2013).
- Whipple, K. X., Hancock, G. S. & Anderson, R. S. River incision into bedrock: mechanics and relative efficacy of plucking, abrasion, and cavitation. *Geol. Soc. Am. Bull.* **112**, 490–503 (2000).
- Granger, D. E., Kirchner, J. W. & Finkel, R. Spatially averaged long-term erosion rates measured from in situ-produced cosmogenic nuclides in alluvial sediment. *J. Geol.* **104**, 249–257 (1996).
- Harel, M.-A., Mudd, S. M. & Attal, M. Global analysis of the stream power law parameters based on worldwide ¹⁰Be denudation rates. *Geomorphology* **268**, 184–196 (2016).
- Gudmundsdottir, M. H. et al. Restraining bend tectonics in the Santa Cruz mountains, California, imaged using ¹⁰Be concentrations in river sands. *Geology* **41**, 843–846 (2013).
- DiBiase, R. A., Whipple, K. X., Heimsath, A. M. & Ouimet, W. B. Landscape form and millennial erosion rates in the San Gabriel Mountains, CA. *Earth Planet. Sci. Lett.* **289**, 134–144 (2010).
- Kirby, E. & Ouimet, W. Tectonic geomorphology along the eastern margin of Tibet: insights into the pattern and processes of active deformation adjacent to the Sichuan Basin. *Geol. Soc. Lond. Spec. Publ.* **353**, 165–188 (2011).
- Harkins, N., Kirby, E., Heimsath, A., Robinson, R. & Reiser, U. Transient fluvial incision in the headwaters of the yellow river, northeastern Tibet, China. *J. Geophys. Res.* **112**, F03S04 (2007).
- Ouimet, W. et al. Regional incision of the eastern margin of the Tibetan Plateau. *Lithosphere* **2**, 50–63 (2010).
- Vance, D., Bickle, M., Ivy-Ochs, S. & Kubik, P. W. Erosion and exhumation in the Himalaya from cosmogenic isotope inventories of river sediments. *Earth Planet. Sci. Lett.* **206**, 273–288 (2003).
- Portenga, E. W. & Bierman, P. R. Understanding Earth's eroding surface with ¹⁰Be. *GSA Today* **21**, 4–10 (2011).
- Lehner, B., Verdin, K. & Jarvis, A. New global hydrography derived from spaceborne elevation data. *Eos* **89**, 93–94 (2008).
- Stock, J. & Dietrich, W. E. Valley incision by debris flows: evidence of a topographic signature. *Water Resour. Res.* **39**, 1089 (2003).
- Sklar, L. S. & Dietrich, W. E. A mechanistic model for river incision into bedrock by saltating bed load. *Water Resour. Res.* **40**, W06301 (2004).

27. Duvall, A., Kirby, E. & Burbank, D. Tectonic and lithologic controls on bedrock channel profiles and processes in coastal California. *J. Geophys. Res.* **109**, F03002 (2004).
28. Shobe, C. M., Tucker, G. E. & Rossi, M. W. Variable-threshold behavior in rivers arising from hillslope-derived blocks. *J. Geophys. Res. Earth Surf.* **123**, 1931–1957 (2018).
29. Rosenbloom, N. A. & Anderson, R. S. Hillslope and channel evolution in a marine terraced landscape, Santa Cruz, California. *J. Geophys. Res.* **99**, 14013–14029 (1994).
30. Wobus, C. W., Hodges, K. V. & Whipple, K. X. Has focused denudation sustained active thrusting at the Himalayan topographic front? *Geology* **31**, 861–864 (2003).

Acknowledgements

G.E.H. acknowledges support from the NSF Career Grant EAR-TECT-105581. G.E.H. and S.P. acknowledge support from the NSF Grant DEB-BIO-0918234. S.P. acknowledges support from the Andrew Mellon Foundation. F.A. acknowledges support from Fondo Nacional de Desarrollo Científico y Tecnológico (FONDECYT-Chile) grant 3150116 and Fondo de Financiamiento de Centros de Investigación en Áreas Prioritarias (FONDAP-Chile), Research Center 15110017.

Author contributions

G.E.H. and S.P. designed the experiment, collected and analysed the samples and wrote the manuscript; G.E.H., F.A., C.W.B., S.A.J., E.L., R.S., A.S. and H.H.Y. participated in the topographic analysis and exploration, contributed to the Supplementary Information and provided feedback on the manuscript text.

Competing interests

The authors declare no competing interests.

Additional information

Supplementary information is available for this paper at <https://doi.org/10.1038/s41561-019-0442-3>.

Correspondence and requests for materials should be addressed to G.E.H.

Reprints and permissions information is available at www.nature.com/reprints.

Publisher's note Springer Nature remains neutral with regard to jurisdictional claims in published maps and institutional affiliations.

© The Author(s), under exclusive licence to Springer Nature Limited 2019

Methods

Erosion rates. We used in situ-produced ^{10}Be in quartz within 14 detrital river sand samples to estimate erosion rates. The 250–500 and 500–710 μm size fractions were extracted from bulk river sand samples, and ~ 100 g of quartz was isolated using magnetic separation followed by progressive HF/HNO₃ leaches. Next, the quartz was digested with ~ 300 μg of Be carrier, and Be was extracted and oxidized to produce BeO₂. $^{10}\text{Be}/^9\text{Be}$ ratios were measured at Lawrence Livermore National Laboratory's Center for Accelerator Mass Spectrometry facility, as well as the Purdue PRIME laboratory. ^{10}Be production rates were corrected for shielding of cosmic radiation by topography³¹, as well as ranges in elevations throughout the basin using the elevation. We used the CRONUS 2.1 online calculator to estimate erosion rates for these samples.

Channel steepness. For collected samples in this study, we calculated channel steepness using the 90-m-resolution CGIAR-SRTM v4 DEM of each sampled site. The model was corrected to ensure hydrologic continuity, and averaged basin steepness was calculated using an integral formulation of steepness described in ref. 13:

$$R_f(x)A_0^\theta = k_s\chi(x) \quad (4)$$

where

$$\chi = \int_{x_b}^x \left(\frac{A_0}{A(X)} \right)^\theta dX$$

where R_f is the fluvial relief measured relative to the reference outlet location (located at x_b), x is the distance from this reference outlet to each point, A_0 is a reference basin area, θ is the concavity and k_s is the channel steepness. Calculation of χ was performed using the derived watershed area at each point using the D8 flow routing algorithm. We used a second-order integration scheme to determine values of χ . R_f was calculated as the elevation drop between each point and the basin outlet¹³. We chose a reference basin area of $A_0 = 1 \times 10^6 \text{ m}^2$, and systematically varied the concavity between 0.4 and 0.6 while regressing $R_f A_0^\theta - \chi$ values to obtain k_s . Relationships between ε and k_s were determined using a piecewise linear orthogonal distance regression of these two values.

For samples drawn from the Portenga and Bierman dataset²³, we filtered samples for basins sampled where little or no morphologic evidence of recent glaciation was present. Next, we isolated all sampled watersheds with basin areas $> 5 \text{ km}^2$, and used the HydroSheds (500-m-resolution) data to calculate steepness as described above. Concavity was varied between 0.4 and 0.6 to explore the effect of its value on k_s .

The difference in spatial resolution between the two datasets raises some questions as to what role the cell dimensions play in biasing estimates of channel steepness. Unlike conventional methods for calculating channel steepness, the integral formulation uses elevation values directly, and so should, in principle, be less impacted by the noise and resolution of the DEM. To explore this potential impact, we analysed each of our sampled basins using 90-m-, 250-m- and 500-m-resolution DEMs of each site. Each of the coarser-resolution datasets was derived from the 90-m-resolution DEM as follows. First, we resampled the 90-m DEM at the reduced resolution using a quintic spline interpolation. Next, we used the priority flooding algorithm³² to fill closed depressions within the basin, and calculated flow routing for this filled DEM using the D8 flow routing algorithm. Finally, we calculated watershed area by sorting the DEM from high to low elevation values, and summing individual pixel contributions to watershed area in the downstream direction. χ and channel steepness values were then calculated for each of these resolutions as before, and the results are listed in Supplementary Table 5.

Interestingly, we found that there are slight, but important biases in the channel steepness values that vary with data resolution. Rather than reducing channel steepness values, where biases existed, the integral method generally resulted in higher channel steepness values as the resolution increased. This resulted from the fact that χ values increase most rapidly within the upper portions of the drainage network for the concavity values used. The effect of increased resolution appeared twofold. First, larger overall cell sizes place limits on the minimum calculated watershed area. Second, and more importantly, large cell sizes tended to produce overall lower catchment areas at the sampled points due to the discretized flow-routing scheme that we used. Both of these factors produced lower χ values for each position in the upstream portions of the basins. As interpolated R_f values are unbiased, this produces a contraction of the χ axis that, according to equation (4), produces higher channel steepnesses. This bias generally decreases with increasing

basin size (Supplementary Table 5), as the range in χ expands for these larger basins and becomes less sensitive to flow routing in the upper portions of the watershed.

Interestingly, this resolution bias helps to explain the small discrepancy between the threshold channel steepness value that we detect using our sampled basins versus the global reanalysis (Supplementary Table 5). In particular, channel steepness values attain a maximum of $\sim 80 \text{ m}^{0.8}$ (for concavity = 0.4), whereas the global compilation shows channel steepness values up to $\sim 112 \text{ m}^{0.8}$ for concavity = 0.4. Interestingly, when downsampling the topographic data for our sample sites to an identical resolution as used in the global compilation, we observed a maximum channel steepness value of $\sim 106 \text{ m}^{0.8}$ for concavity = 0.4. Thus, the lower channel steepness threshold observed in our data relative to the maximum steepness value observed in the global compilation is consistent with the expected upward bias in channel steepness for the coarser resolution data.

We calculated the global distribution of k_s by identifying and regressing (χ , R_f) values along channel segments. k_s was computed using (χ , R_f) values extracted along a segment that runs up- and downstream from, and is centred on, each cell of interest in the DEM. The span of this segment varies horizontally in a way that achieves a specified vertical elevation drop across each channel segment. This methodology acknowledges the fact that noise in DEM elevations may produce higher misfits of (χ , R_f) regressions in low-relief, large catchment areas when using a path of fixed horizontal extent. Locations that define each segment are identified as follows. Flow paths located upstream of the point of interest were selected on the basis of the path that adheres to the upstream flow routing, while tracking the route that maximizes the watershed area draining to each point. This dual condition is required because the D8 flow routing used here³³ allows multiple cells in the DEM to drain to a common downstream cell. Those points lying downstream were identified by the flow routing, since each upstream cell drains to a single downstream cell. Starting from each point at which k_s is to be calculated, we incrementally searched an equal number of points up- and downstream, using the protocol described above. We incremented the number of cells along the flow path symmetrically about the target cell until the specified elevation drop, herein conservatively set to 48 m, was reached or exceeded. A value of 48 m was used because it is 3 times the design target for vertical precision of the source data from which the HydroSheds DEM is derived³⁴. Once the cells along the path were found, χ and R_f values were calculated for each cell, from bottom to top. Equation (4) was evaluated for each point along the profile using the trapezoidal rule. Linear regression was then used to calculate the k_s value at the midpoint of this path, its value was recorded with the number of points along the flow path and the number of times each adjacent cell participates in a k_s calculation, and the process was repeated for all cells in the DEM. Unbiased probability density and cumulative distribution functions (CDFs) of k_s were generated by unweighting the cumulative distributions according to the number of times each cell was used in calculating an adjacent k_s value. These cumulative distributions were then used to estimate the fraction of points falling below specified k_s values. The use of a fixed vertical interval excludes the upper portions of basins whose elevation drop is less than 48 m, which tends to concentrate k_s measurements in steep portions of landscapes relative to low-relief catchments. This biases the CDFs towards higher values, which provides a maximum upper bound on the CDFs of k_s . Himalayan points were isolated as those lying in the ranges $83^\circ \text{ E} - 94^\circ \text{ E}$ and $27^\circ \text{ N} - 30.5^\circ \text{ N}$.

Data availability

The authors declare that all data supporting the findings of this study are available within the article, its Supplementary Information and at <https://doi.org/10.25740/vp967gh7489>.

Code availability

The code to reproduce the results of this work can be accessed at <https://github.com/stgl/GlobalSteepness> and <https://github.com/stgl/TopoAnalysis>.

References

1. Moon, S. et al. Climatic control of denudation in the deglaciated landscape of the Washington Cascades. *Nat. Geosci.* **4**, 469–473 (2011).
2. Barnes, R., Lehman, C. & Mulla, D. Priority-flood: an optimal depression-filling and watershed-labeling algorithm for digital elevation models. *Comput. Geosci.* **62**, 117–127 (2014).
3. O'Callaghan, J. F. & Mark, D. M. The extraction of drainage networks from digital elevation data. *Comput. Vis. Graph. Image Process.* **28**, 323–344 (1984).
4. Farr, T. G. et al. The shuttle radar topography mission. *Rev. Geophys.* **45**, RG2004 (2007).